The Thresholds of Urban Parks' Characteristics on Heat Mitigation EffectβCase Study of 120 Parks in Foshan, China

Lihua Chen, Jing Gan
Affiliation: College of Architecture and Urban Planning, Tongji university
Email: 2410354@tongji.edu.cn; jinggan@tongjing.edu.cn

Abstract
In the context of the increasingly severe global thermal environmental crisis, this paper examines 120 urban parks in Foshan, a representative water-network city in China's southern region. By using multi-methods integrating Boosted Regression Tree (BRT) modeling, Restricted Cubic Spline (RCS) threshold detection, and K-means clustering, the study explores cooling effectiveness of urban parks based on five metrics: Park Cooling Distance (PCD), Park Cooling Area (PCA), Park Cooling Efficiency (PCE), Park Cooling Intensity (PCI), and Park Cooling Gradient (PCG). Results reveal threshold-dependent cooling effects, with park area, blue-green ratio, and FAR as key determinant factors. Thresholds for optimal cooling efficiency occur at 2.31-4.03 km² park area, vegetation coverage exceeding NDVI 0.277, and blue-water ratio within 0.277-0.515. All the sampling parks could be clustered into four groups: high-efficiency, low-efficiency, medium-efficiency, and comprehensive cooling performance. The findings could provide reference to deeply understand the threshold mechanism in urban heat mitigation and evidence-based planning strategies for optimizing green infrastructure in water-network cities, supporting science-driven thermal environment optimization.

Keywords: Urban Heat Island Effect; Urban Parks; Green Infrastructure; Cooling Mechanism; Lingnan Water Network Cities

1. Introduction

1.1 Urban Heat Island Crisis and the Climate Regulating Role of Green Spaces

With the acceleration of global urbanization, the Urban Heat Island (UHI) effect has become an important environmental issue that threatens the health of urban ecosystems and the well-being of residents. (Oke & Maxwell, 1975; Rizwan et al., 2008). According to the 2021 IPCC report, urban surface temperatures in the 21st century have increased by 1.5-3.0°C compared to the pre-industrial period, with a significant increase in the frequency of extreme heat events (Masson-Delmotte et al., 2021). Urban green spaces have become a central vehicle for heat island mitigation through transpiration, shade effect and air flow regulation (Gong et al., 2024). A properly planned urban park can reduce the surrounding surface temperature by 1-5°C, and its cooling effect is closely related to the characteristics of park area, vegetation cover, and proportion of water bodies (GALLO et al., 1993; Kayet et al., 2016). However, the synergistic cooling mechanism of blue-green spaces in cities with dense water networks is not clear (Stewart, 2011; Zhang et al., 2024).

1.2 Thermal Environment Specificity of Lingnan Water-Network Cities

The Lingnan region is one of the fastest urbanising regions in China, with average annual temperatures 2-3°C higher than the national average and 60-90 days of high temperature in summer (Z. Yu et al., 2017). Foshan is located in the Pearl River Delta and is a typical water network city in the Lingnan region, with a hydrological pattern of the three river confluences of the West River, North River, and Sui River. Foshan has a river density of 0.8-1.2 km/km², creating a unique landscape of a water network city (Foshan Municipal People's Government, 2025). However, rapid urbanisation has led to fragmentation of green spaces and pollution of water bodies, weakening the synergistic cooling capacity of blue-green spaces (Gago et al., 2013). The cooling effect of water network urban parks is multiply affected by the distribution of water bodies, the structure of green space and the intensity of surrounding development (Bowler et al., 2010; Yang et al., 2020). However, studies addressing the threshold effect of their blue-green spaces still need to be supplemented.

1.3 Contradiction Between Threshold Deficiency and Planning Demands

Currently, urban green space planning faces challenges in the context of UHI. It is difficult to quantify the spatial cooling range and intensity of parks without comprehensive cooling performance indicators (Chang & Li, 2014; Feyisa et al., 2014). Measuring marginal effects and identifying thresholds for influencing factors such as park area and blue-green space need further research (Oliveira et al., 2011; Z. Yu et al., 2020). Local planning guidelines lack targeted strategies, leading to inefficient layout of blue-green spaces in water network cities (Ministry of Housing and Urban-Rural Development, 2020). Therefore, there is an urgent need to construct a complete framework of 'Indicators - Mechanisms - Thresholds - Strategies' to provide a scientific basis for thermal mitigation planning in water network cities.

1.4 Research Objectives and Innovations

In this study, 120 parks in Foshan City were used to quantify the spatial cooling effect of the parks by introducing five major indicators, namely PCD (park cooling distance), PCA (park cooling area), PCE (park cooling efficiency), PCI (park cooling intensity), and PCG (park cooling gradient). The non-linear relationship is resolved by identifying the marginal thresholds of factors such as scale, landscape pattern, blue-green space and the surrounding built environment. Finally, based on the k-mean clustering results, optimisation strategies are proposed for four different types of parks with different cooling performance. This study aims to reveal the mechanism of the cooling effect of water network city parks, provide a scientific basis for the optimisation of blue-green space layout, and contribute to the sustainable development of water network cities under the background of global climate change.

2. Materials and methods

2.1. Study area

This study took Foshan City (23°02'N-23°24'N, 112°51'E-113°23'E) as the study area, with a total area of 3797 km², which has a southern subtropical monsoon climate, with an average temperature of 28.5°C in summer (June-August), and extreme high temperatures of up to 39.2. The total length of urban rivers exceeds 6000 km, and the density of the river network is 1.58 km/km². In this study, 120 representative parks were selected from the screening of 382 parks larger than 1 ha. According to the park classification standard of Foshan City, the 120 parks cover five categories: community parks (36%), comprehensive parks (20%), wetland parks (8%), forest parks (12%), and special parks (24%).

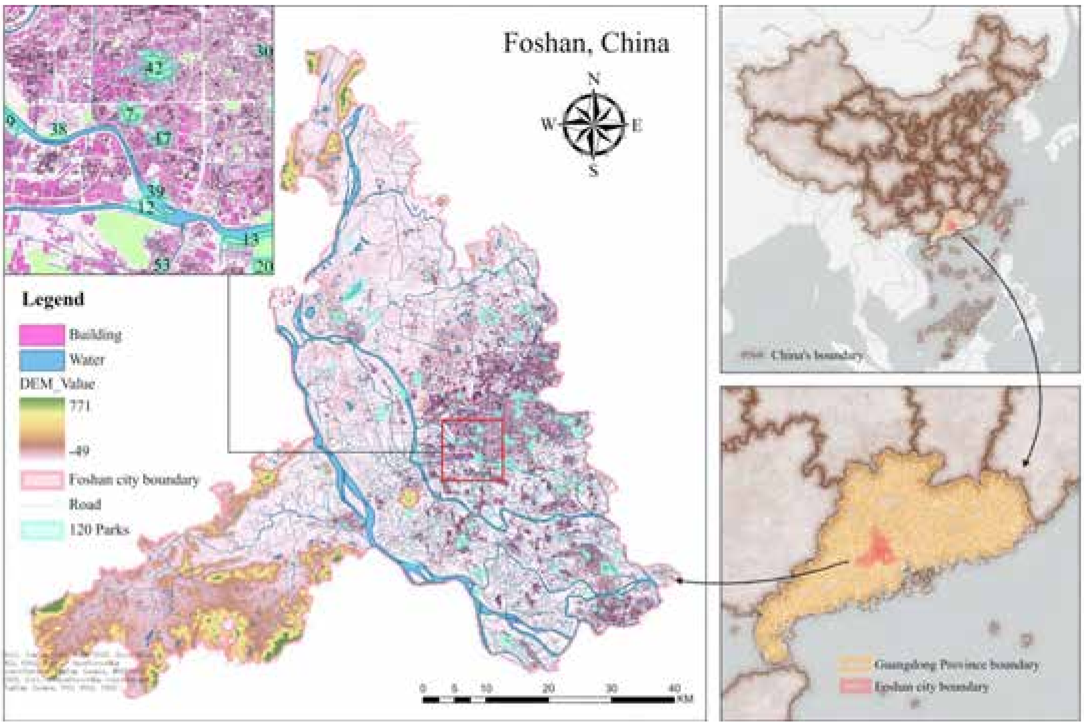

Figure 1 Distribution of the study area and 120 parks in Foshan City (Base map is from the standard map downloaded from the website of the Standard Map Service of the Ministry of Natural Resources (http://bzdt.ch.mnr.gov.cn/))

2.2 Data Sources

2.2.1 Inversion of Surface Temperature

This study used the radiative transfer equation method to invert land surface temperature (X. Yu et al., 2014) providing two adjacent thermal bands, which has a great benefit for the LST inversion. In this paper, we compared three different approaches for LST inversion from TIRS, including the radiative transfer equation-based method, the split-window algorithm and the single channel method. Four selected energy balance monitoring sites from the Surface Radiation Budget Network (SURFRAD. The basic principle involves estimating atmospheric effects on surface thermal radiation, subtracting them from the total thermal radiation observed by satellite sensors to get surface thermal radiation intensity, and then converting it to land surface temperature.

$$L\lambda = [\varepsilon B(Ts) + (1 - \varepsilon) L\text{-}]\tau + L\text{-}$$

L∆is the thermal infrared radiation brightness observed by the satellite sensor; L∆is atmospheric upwelling radiance; L∆is the energy from atmospheric downwelling radiance reflected back after reaching the ground; B(Ts) is blackbody thermal radiation brightness; ∆is atmospheric transmittance in the thermal infrared band. L∆ L∆ and ∆were obtained from the NASA website (http://atmcorr.gsfc.nasa.gov/). ∆is land surface emissivity, calculated using the NDVI threshold method by Sobrino (Sobrino et al., 2004)three methods to retrieve the land surface temperature (LST. Ts is the actual land surface temperature.

$$Ts = K2 / \ln[K1 / B(Ts) + 1]$$

For Landsat - 8, K1 = 774.89 W/(m²·sr·μm) and K2 = 1321.08 K.

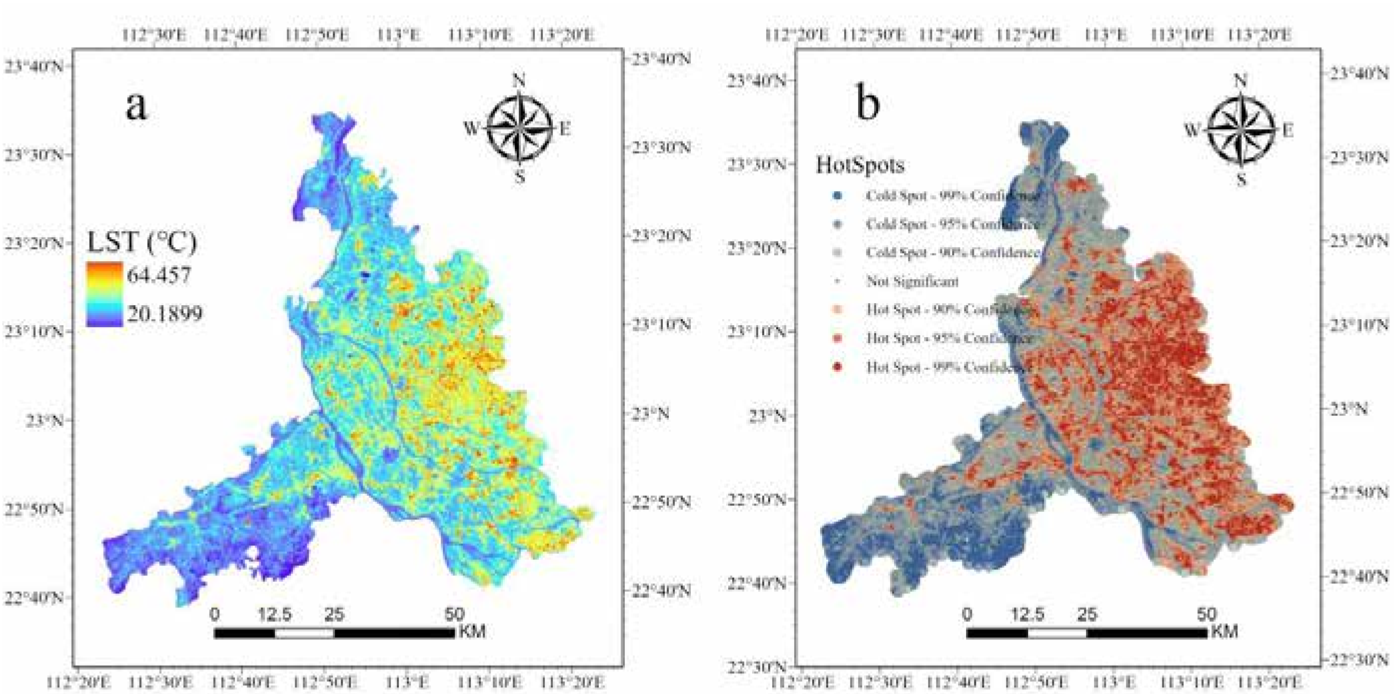

Figure 2 Mean surface temperature of the study area (a) and hotspot analysis map (b). (LST inversion in September 2022)

2.2.2 Data Sources

Remote sensing monitoring data, geospatial data, meteorological observation data and land use data were used in this study (Table 1). The surface temperature (LST) data were obtained from Landsat 8 OLI/TIRS satellite imagery, which was selected during the cloud-free period of September in the summer of 2022, and radiolabelled, atmospherically corrected, and inverted by the single-window algorithm to obtain the surface temperature distribution (Jimenez et al., 2010)thermal imagery at medium and high spatial resolution is useful in many environmental studies, such as evapotranspiration estimation from the energy balance equation, which is a key parameter when working in water resources management. In this sense, the launch in 1982 of the Thematic Mapper (TM. In addition, the field validation was carried out in September 2022, and the surface temperatures of 50 sample points were collected by portable infrared thermometers. Comparison with the satellite inversion results showed that the root mean square error (RMSE) was 1.2°C, and the absolute error was controlled within 1.5°C. The high resolution remote sensing images were collected using the GIS and the GIS. The high-resolution remote sensing image adopts GF-2 satellite data, and after orthorectification, image fusion and Support Vector

Machine (SVM) feature classification, it realises the interpretation of the landscape elements such as forest, grassland, water and impermeable surface of the park.

Table 1 Data Sources

Data Type	Source	Time Range	Preprocessing Methods
Surface Temperature (LST)	Landsat 8 OLI/TIRS (30 m)	Summer 2022 (September)	Radiometric calibration → Atmospheric correction (MODTRAN model) → Single-window algorithm inversion (Jiménez-Muñoz & Sobrino, 2003)
Remote Sensing Imagery	GF-2 Satellite (2 m)	July 2023	Orthorectification → Image fusion → Land cover classification (Support Vector Machine, SVM)
Park Vector Data	Foshan Natural Resources Bureau	2023	Boundary vectorization → Topological inspection → Attribute assignment (area, type, water body proportion, etc.)
Meteorological Data	Foshan National Benchmark Climate Station	2018–2023	Interpolation to generate 1 km resolution raster data (ANUSPLIN model)
Land Use Data	Guangdong Provincial Land Use Status Database	2022	Reclassification into 7 categories including construction land, green space, and water bodies (GB/T 21010–2017)

2.3 Methodology

2.3.1 Quantification of Park Cooling Performance

In this study, the ArcGIS multi-ring buffer model was used to quantify the spatial gradient changes and further quantify the attenuation pattern of the land surface temperature (LST) during the outward extension of the park boundary. A buffer zone is set every 30 metres from the park boundary, generating 40 concentric buffer zones covering a 1200-metre buffer zone. The buffer zone model is based on the Sanshan Forest Park, where the interior of the park is dark green, the area affected by the park cooling is mauve, and the unaffected area is yellow.

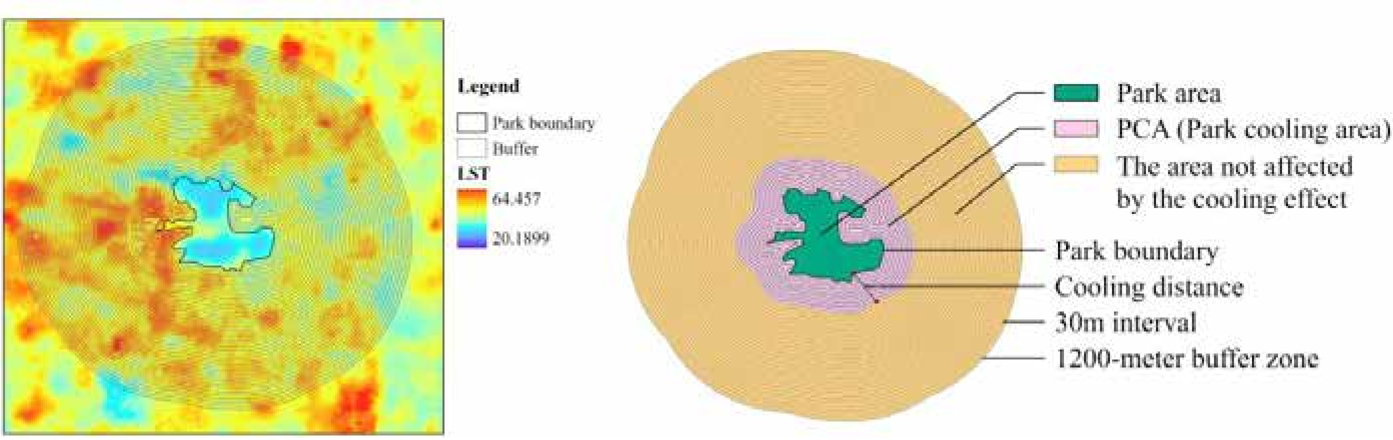

Figure 3 Schematic diagram of multi-ring buffer analysis (taking Sanshan Forest Park as an example, with 30 buffers extending to 1,200 m)

In order to quantify the thermal mitigation effect of the park on the city and to analyse the changing pattern of the park's cooling of the surrounding environment, this study fits a decay curve of the park's LST with distance from the park boundary. As shown in Fig. 4, the variation of buffer LST over the 1200 m buffer distance range of the park is depicted. The park temperature is at the starting point and represents the baseline average temperature within the park. As the distance increases, the average LST per 30 metre buffer goes from increasing to levelling off. The first turning point on the curve is a key metric that calculates park cooling intensity PCI and park distance distance PCD (Aram et al., 2019)..

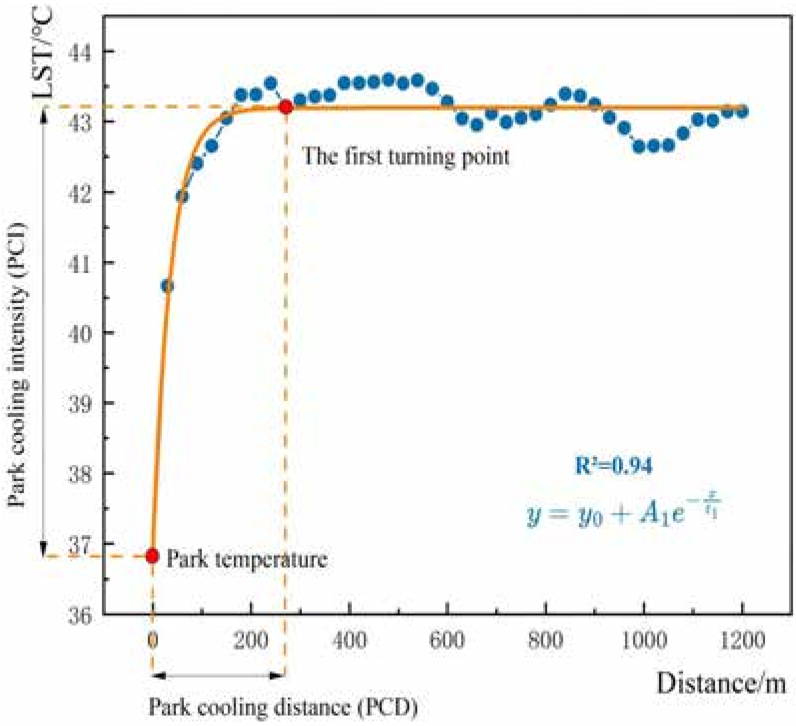

Figure 4 Curve fit of park thermal mitigation to the surroundings (average LST trend per 30 m buffer outside the park, in the case of Sansan Forest Park)

The park cooling effect evaluation system incorporates a multi-dimensional framework comprising five key metrics (Table 2): Park Cooling Distance (PCD), Park Cooling Area (PCA), Park Cooling Efficiency (PCE), Park Cooling Intensity (PCI), and Park Cooling Gradient (PCG). These indicators collectively provide a comprehensive quantification of urban parks' thermal mitigation capacity .

Table 2 Evaluation Index System for Park Thermal Mitigation Effects

Indicator	Definition	Calculation Formula	Unit
Park Cooling Distance (PCD)	Distance from park boundary to the boundary of the cooling effect	PCD = Distance from the first turning point to the park boundary (Figure 4)	m
Park Cooling Area (PCA)	Area within the park's influence range where temperature is significantly lower than the background value	PCA = Area of the buffer zone from the first turning point to the park boundary	km^2
Park Cooling Efficiency (PCE)	Cooling area per unit park area	PCE = PCA / Park area	km^2/km^2
Park Cooling Intensity (PCI)	Average temperature drop within the cooling range	PCI = ΔT (Buffer zone LST - Park LST)	
Park Cooling Gradient (PCG)	Attenuation rate of temperature drop with distance from the park	PCG = ΔT / Distance	100m

2.3.2 Selection of Environmental Variables

In order to reveal the key drivers of thermal mitigation effects in urban parks, 20 variables were selected in this study from six dimensions: park morphology, distribution, structure, surrounding built environment, peripheral land cover and regional climate (Table 3). The first three dimensions are within the park, and the last three dimensions are located outside the park within the 1200 m buffer zone.

Table 3 Definitions and Calculation Methods of Influence Variables

Indicator Category	Specific Indicator	Abbreviation	Formula
Park Morphological Features	Park Area	PA	Vector data area
	Park Perimeter	PP	Vector data perimeter
	Elevation	DEM	Mean elevation within the park
	Normalized Difference Vegetation Index	NDVI	$NDVI = \frac{NIR - R}{NIR + R\text{w}}$
Park Distribution Features	Impervious Surface Area Ratio	BR	$BR = \frac{\text{Impervious Surface Area in Park}}{\text{Total Park Area (PA)}}$
	Water Area Ratio	WR	$WR = \frac{\text{Water Body Area in Park}}{\text{Total Park Area (PA)}}$
	Forest Area Ratio	FR	$R = \frac{\text{Forest Land Area in Park}}{\text{Total Park Area (PA)}}$
	Grassland Area Ratio	GR	$GR = \frac{\text{Grassland Area in Park}}{\text{Total Park Area (PA)}}$
Park Structural Features	Landscape Shape Index	LSI	$SI = \frac{\text{Park Perimeter (PP)}}{2\sqrt{\pi} \times \text{Park Area (PA)}}$
	Aggregation Index	AI	$AI = \frac{\sum_{i=1}^{n} \sum_{j=1}^{n} a_{ij}}{A} \times 100$
	Contagion Index	CONTAG	$CONTAG = 100 \times \frac{-\sum_{i=1}^{n} \sum_{j=1}^{n} p_{ij} \ln(p_{ij})}{2\ln(n)}$
Built Environment Surrounding	Building Density	BD	$BD = \frac{\text{Building Base Area}}{\text{Site Area}} \times 100\%$
	Floor Area Ratio	FAR	$FAR = \frac{\text{Total Floor Area}}{\text{Site Area}}$
Land Cover Surrounding Parks	Impervious Surface Ratio in Buffer	BBR	$BBR = \frac{\text{Impervious Surface Area in Buffer}}{\text{Total Park Area (PA)}}$
	Water Body Ratio in Buffer	BWR	$BWR = \frac{\text{Water Body Area in Buffer}}{\text{Total Park Area (PA)}}$
	Forest Ratio in Buffer	BFR	$BFR = \frac{\text{Forest Land Area in Buffer}}{\text{Total Park Area (PA)}}$
	Grassland Ratio in Buffer	BGR	$BGR = \frac{\text{Grassland Area in Buffer}}{\text{Total Park Area (PA)}}$
Climatic Conditions Surrounding	Surrounding Temperature	BLST	Mean LST in buffer zone
	Surrounding Wet	BWET	Mean humidity in buffer zone
	Surrounding Elevation	BDEM	Mean DEM in buffer zone

2.3.3 Analysis Models

(1) **Boosted Regression Tree (BRT) Model**

This study employed the Boosted Regression Tree (BRT) model to quantifie the influence of independent variables on dependent variables through relative Influence. This approach integrates multiple regression trees through a machine learning strategy to effectively capture complex interactions and threshold effects among variables (Elith et al., 2008; Friedman, 2001). The model's predictive accuracy was validated using the root-mean-square error (RMSE) and coefficient of determination (R^2) to ensure its reliability in quantifying the thermal effects of urban parks, providing data-driven support for subsequent spatial planning strategies.

$$RI_v = \frac{\sum_{m=1}^{M} \sum_{k=1}^{K_m} \Delta E_{m,k,v}}{\sum_{m=1}^{M} \sum_{k=1}^{K_m} \Delta E_{m,k}} \times 100\%$$

Where "v" is target independent variable (e.g., NDVI, BD); "M" is total number of regression trees; "K_m" is number of splits in the m-th tree; is reduction in squared error when variable v is used in the k-th split of the m-th tree.

(2) Restricted Cubic Spline (RCS) Curves and Threshold Identification

Restricted Cubic Spline (RCS) is a nonparametric statistical method that fits the nonlinear relationship between a continuous variable and a response variable by means of a segmented cubic polynomial function, with first and last linear constraints imposed to ensure the smoothness of the curve and the stability of the extrapolation (Govindarajulu et al., 2009; Zhao et al., 2024). The core advantage of RCS is its ability to automatically capture complex nonlinear patterns through segmental fitting and smooth connections. Its mathematical form is as follows.

$$f(X) = \beta_0 + \beta_1 X + \sum_{k=1}^{K-2} \beta_{k+1} \cdot h_k(X)$$

X is a continuous predictor variable; hk is the basis function; and tk is knots, usually taken as equidistant quartiles. In order to identify the thermal mitigation thresholds of the parks for the urban environment, the first order derivative (slope) and second order derivative (curvature) of the curves were calculated.The RCS curves allow for the identification of two critical inflection points (Fig. 5). The two critical inflection points are defined in the first-order derivative plot as the point where the slope of threshold 1 (T1) is 0 and threshold 2 (T2) is the point with the largest slope, when the rate of thermal mitigation of the park to the urban environment is likely to be optimal.

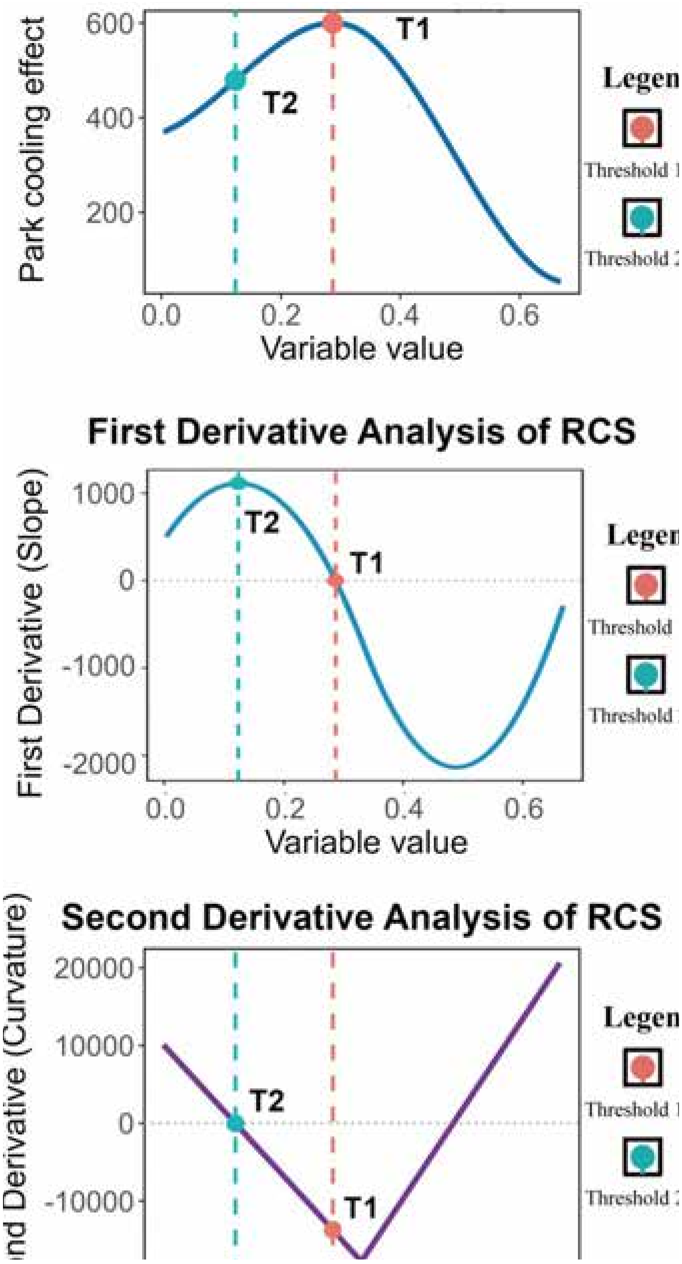

Figure 5 Schematic Diagram of Restricted Cubic Spline (RCS) and Thresholds

(3) K-means Cluster Analysis

In this study, a K-means clustering algorithm was used to classify the cooling performance of parks, with the aim of identifying clusters with similar cooling characteristics and quantifying their relative contributions (Kanungo et al., 2002)we are given a set of n data points in d-dimensional space R/sup d/ and an integer k and the problem is to determine a set of k points in Rd, called centers, so as to minimize the mean squared distance from each data point to its nearest center. A popular heuristic for k-means clustering is Lloyd's (1982. The optimal number of clusters was determined by the elbow rule in conjunction with the contour coefficient method. The elbow rule is based on the inflection point of the curve of the within-group sum of squares (WSS) with respect to the number of clusters, and the contour coefficient method is performed by calculating the average contour coefficient of 2 to 10 clusters (with values ranging from [-1,1], with larger values indicating better intra-cluster compactness and inter-cluster separation. The final result is determined (K = 4) as the optimal number of clusters.

3. Research Results

3.1 Spatial Patterns of Park Thermal Mitigation in Summer

3.1.1 Gradient Attenuation of Cooling Performance

In the spatial pattern of heat mitigation in parks in summer, the gradient decay of cooling effect showed significant regularity and spatial differentiation characteristics. Based on the buffer zone temperature analysis, all parks formed a significant cooling zone, with a mean park cooling distance (PCD) of 493.5 m and a mean cooling intensity (PCI) of 3.7 °C. The park cooling gradient (PCG) was 1.38°C/100 m, which means that the temperature drop decreased by 1.38°C with every 100 m increase in distance from the park, revealing the basic law that the park thermal mitigation effect exponentially decays with increasing spatial distance. The analysis of spatial heterogeneity shows that there are significant differences in cooling efficiency and coverage between parks of different zones and sizes. Wetland parks in the suburbs (e.g., Yundonghai Wetland Park in Sanshui, with an area of 4.35 km²) had a park cooling area (PCA) of 6.21 km² and a park cooling efficiency (PCE) of 1.43 km²/km², while community parks in the city centre (e.g., Zhongshan Park in Chancheng, with an area of 0.27 km²) had a PCA of only 1.58 km², but their PCE was as high as 5.72 km²/km². This suggests that although small parks have advantages in cooling efficiency, their absolute cooling coverage is limited due to their size (Figure 6).

The modulation of the cooling effect by the heat island background is significant. The mean surface temperature (LST) in the city centre area (Chancheng District) is 40.88°C, which is 7.3°C higher than that in the suburban area (Gaoming District), and as a result, the cooling gradient (PCG) in the city centre parks is 0.97°C/100 m, which is significantly lower than that in the suburban parks, which is 1.61°C/100 m. (Fig. 7), which suggests that the spatial decay rate of the cooling effect of the parks is weakened by the high intensity of the heat island environment. This indicates that the high-intensity heat island environment will weaken the spatial decay rate of the cooling effect in the parks, forming a spatial pattern of slowing down the cooling gradient in the thermal background.

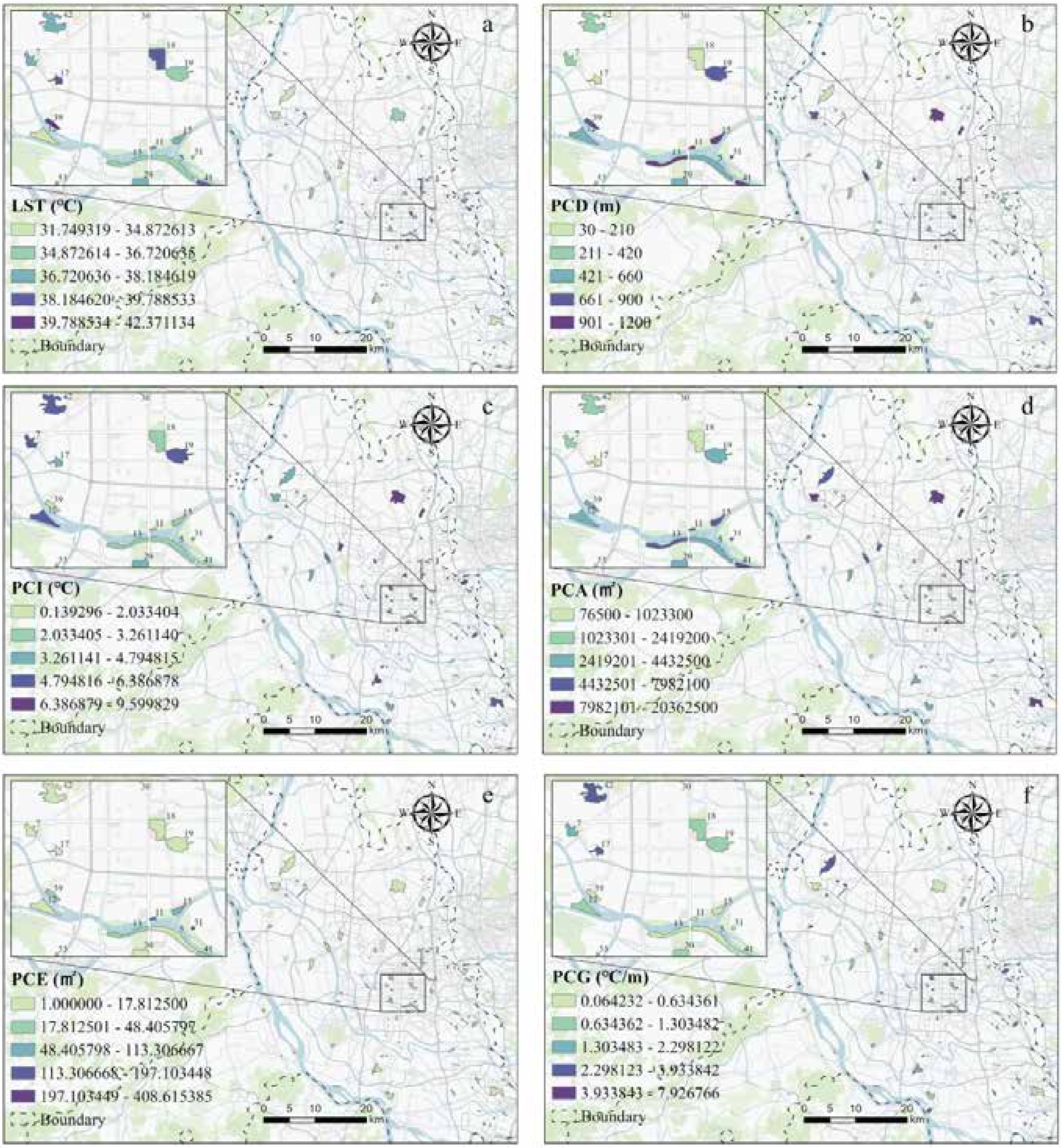

Figure 6 Spatial Distribution Maps of LST and 5 Park Cooling Performance Index for 120 Urban Parks: (a) Park LST, (b) PCD index, (c) PCI index, (d) PCA index, (e) PCE index, (f) PCG index.

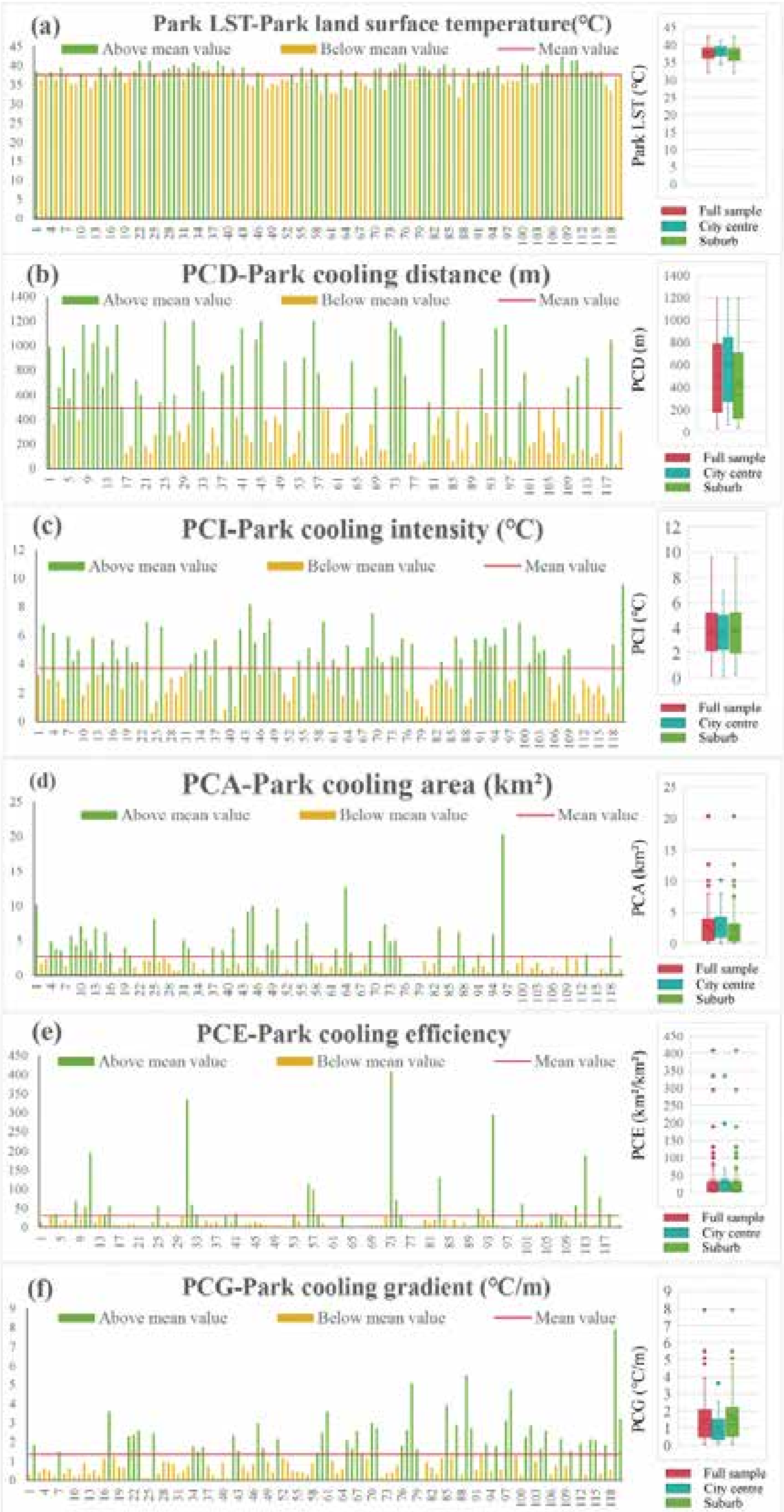

Figure 7 Bar Charts and Boxplots of Six Cooling Indices for 120 Urban Parks: The red boxplots represent the full sample, light green denotes downtown areas, and dark green indicates suburban areas.

3.1.2 Cooling Performance of Different Park Types

Based on the Foshan City park classification standard, the 120 parks included Community Parks, Comprehensive Parks, Wetland Parks, Forest Parks, and Special Parks. Among them, Forest Parks had an average PCI of 5.44±1.61°C, which was significantly higher than that of other types of parks, and their average PCA (4.84±5.38 km^2) and PCG (1.8±1.4°C/100m) were higher compared with those of other parks, which was attributed to the synergistic effect of their large natural vegetation and complex ecosystems.Comprehensive Parks' PCA (4.36±3 km^2) and PCD (743.75±287.75m), were outstanding, possibly due to their diverse landscaping with a large footprint. In contrast, the average PCI of specialised parks was only 2.23±1.62°C, but their PCE (43.58±98.84 km^2/km^2) showe1d high discrete characteristics, reflecting the differences in design elements such as vegetation configurations and water body areas in different specialised parks. Although the wetland park had a higher PCG (1.66±0.95°C/100m), its PCA was smaller (1.11±2.92 km^2), which might be limited by the localised evapotranspiration of wetland water bodies.

Table 4 Cooling Performance of Different Park Types

Park Type	Sample	Mean PCI/℃	Mean PCA/ km^2	Mean PCE/km^2/ km^2	Mean PCD/m	Mean PC-G/℃/100m
Community Parks	43	3.71±1.48	2.69±1.35	30.21±35.59	493.5±260.8	1.38±0.82
Comprehensive Parks	24	4.08±2.01	4.36±3	40.84±61.52	743.75±287.75	0.68±0.61
Wetland Parks	10	4.05±1.59	1.11±2.92	23.28±15.57	337.67±409.19	1.66±0.95
Forest Parks	14	5.44±1.61	4.84±5.38	11.49±18.72	555±414.32	1.8±1.4
Special Parks	29	2.23±1.62	1.81±1.81	43.58±98.84	393.1±380.09	1.56±1.88

3.2 Key Influencing Factors of Park Cooling Performance

3.2.1 Significance ranking of the Variables

Based on the BRT model results (Fig. 8), the model fit was generally satisfactory, with PCD (R^2=0.64), PCA (R^2=0.87), PCE (R^2=0.58), PCG (R^2=0.67), and PCI (R^2=0.83). Landscape pattern, land cover type, park morphological features and built environment were the core influences on thermal mitigation. Among them, in PCA, Park Perimeter (PP) was the most critical, reflecting the influence of park morphological boundaries on cooling diffusion, and Park Morphological Features accounted for 27.74%, indicating that the park's own morphological structure was the core factor determining PCA; on Cooling Efficiency (PCE), the importance of Park Area (PA) was prominent, showing that the scale effect had an impact on the cooling efficiency of unit area. Land Cover Types and Park Morphological Features together accounted for 81.98%.

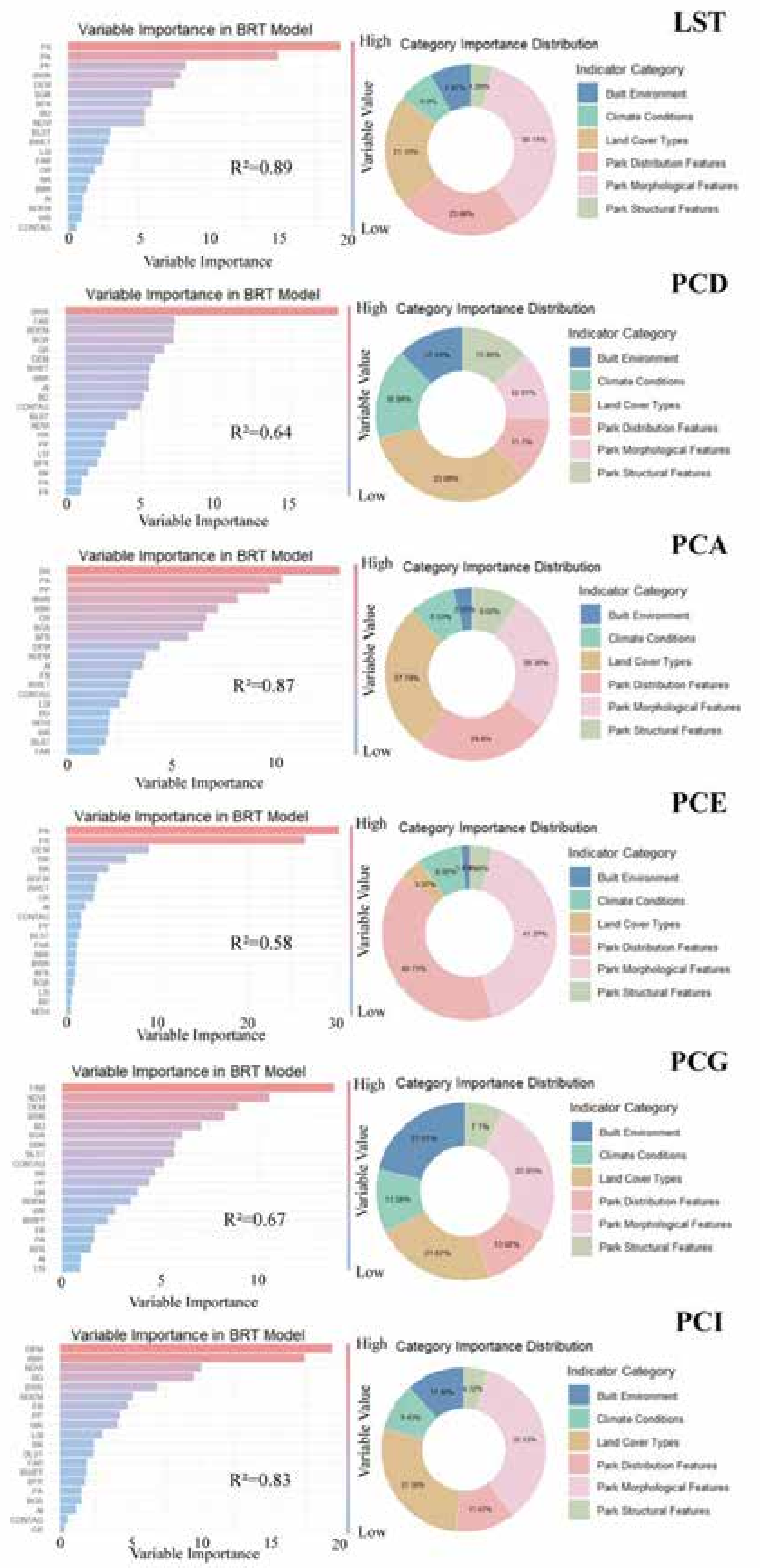

Figure 8 Importance Ranking of Influence Variables on Park Cooling Performance Based on BRT Model

3.2.2 Marginal Effect Analysis

Based on the BRT model, the study selected the five influencing variables with the highest variable ranking, constructed their restricted cubic spline curves (RCS curves) with the five park cooling performance indices (PCD, PCA, PCE, PCG, and PCI), and identified the thresholds (Figure 9). The park cooling performance index is mainly affected by various factors such as PA, DEM, FAR, NDVI, BD, BBR, BWR, etc., and shows a complex nonlinear relationship. Using the RCS curve, we can explore the increase and decrease of cooling intensity when the values of variables change, so as to guide the reasonable use of relevant variables to improve cooling intensity in park design, and then assist in determining the scope of variable control to improve cooling efficiency.

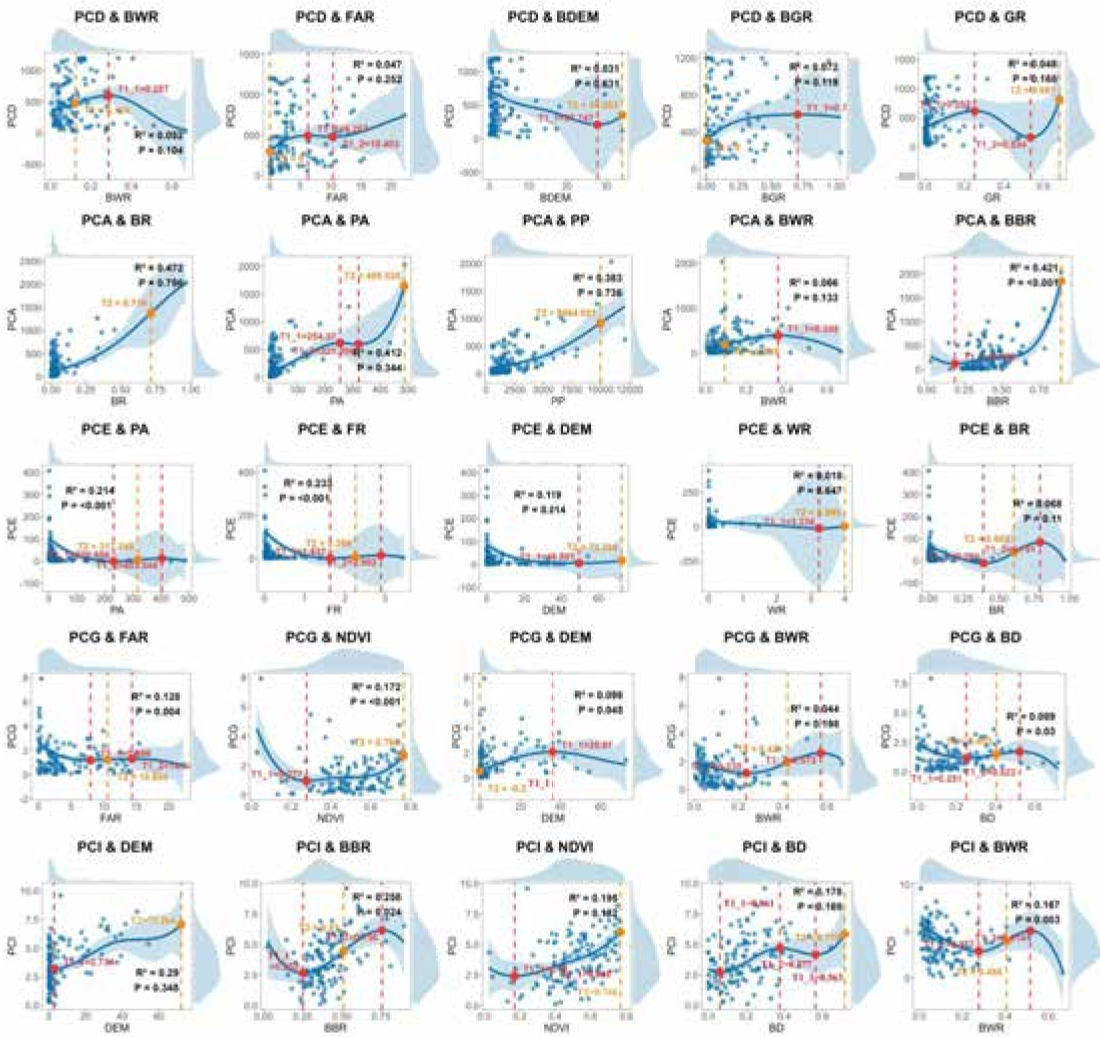

Figure 9 Restricted Cubic Spline (RCS) Curves and Threshold Identification for the Top Five Influencing Variables Ranked by the BRT Model and Five Park Cooling Performance Indices (Thresholds Marked in Yellow as T2 and Red as T1)

3.3 Threshold of Heat Mitigation Effects

Based on the RCS curve model, statistically significant thresholds were identified for 8 key variables (Table 5). Park area (PA) (R2 = 0.214, P < 0.001) showed increasing marginal utility of PCE in the interval [2.31, 4.03] k m^2, with the fastest growth rate at 3.17 k m^2, suggesting that moderately sized parks are favourable for the improvement of cooling efficiency.In terms of DEM, the effects on PCE (R2 = 0.119, P < 0.05) and PCG (R^2 = 0.098, P < (R^2=0.098, P<0.05) varied at different thresholds, with PCE changing from decreasing to increasing when the threshold exceeded 49.551m. Among the indicators of the built environment around the park, the building density (BD) (R^2=0.089, P 0.05) showed an increasing trend in the interval of [0.251, 0.523], and the fastest rate of change was observed at 0.403; the floor area ratio (FAR) (R^2=0.128, P 0.01) showed an increasing trend in the interval of [7.986, 14.34], and the slope of increase was observed at 10.604, and the slope of increase at 10.604. The slope of the increase reached its maximum at 10.604. The NDVI (R^2=0.172, P<0.001), an indicator of vegetation cover, showed an increasing trend of PCG in the interval of [0.277, 0.766], with the maximum slope at 0.766. BBR (R^2=0.167, P<0.05) and BWR (R^2=0.167, P<0.05), positively affected PCA and PCI in the intervals [0.252, 0.756] and [0.277, 0.516], respectively, and reached the extremes of the rate of increase at the 51% and 40% thresholds.

Table 5 Thresholds of Key Variables for Cooling Performance and Their Ecological Significance

Variable	Cooling Performance Index	Threshold	Physical Meaning	Significance
PA	PCE	T1_1=2.31 km², T1_2=4.03 km²	When PA is within [2.31, 4.03] km², per-unit cooling efficiency (PCE) shows an upward trend (increasing marginal utility); outside this interval, PCE declines (decreasing marginal utility).	R^2=0.214, P < 0.001
		T2=3.17 km²	At PA=3.17 km², the slope reaches its peak, indicating the fastest growth rate of PCE.	
DEM	PCE	T1=49.551 m	Below 49.551 m, PCE decreases rapidly with elevation; above 49.551 m, PCE increases.	R^2=0.119, P < 0.05
		T2=72.266 m	At 72.266 m, the growth rate of PCE reaches its maximum.	
	PCG	T1=35.97 m	Below 35.97 m, PCG rises rapidly with elevation; above 35.97 m, PCG declines.	R^2=0.098, P < 0.05
FAR	PCG	T1_1=7.986, T1_2=14.34	When FAR is within [7.986, 14.34], PCG shows an upward trend; outside this interval, PCG declines.	R^2=0.128, P < 0.01
		T2=10.604	At FAR=10.604, PCG increases at the fastest rate.	
NDVI	PCG	T1=0.277	Below NDVI=0.277, PCG decreases with NDVI; above 0.277, PCG increases. This marks the transition point from decline to growth.	R^2=0.172, P < 0.001
		T2=0.766	Within NDVI [0.277, 0.766], PCG rises; at NDVI=0.766, the growth rate peaks.	
BD	PCG	T1_1=0.251, T1_2=0.523	Within BD [0.251, 0.523], PCG increases; outside this range, PCG decreases.	R^2=0.089, P < 0.05
		T2=0.403	At BD=0.403, the rate of PCG change reaches its maximum.	
BBR	PCA	T1=0.188	Below BBR=0.188, PCA decreases with BBR; above 0.188, PCA increases. This marks the transition from decline to growth.	R^2=0.421, P < 0.001
		T2=0.896	At BBR=0.896, PCA increases at the fastest rate.	
BBR	PCI	T1_1=0.252, T1_2=0.756	Within BBR [0.252, 0.756], PCI increases; outside this range, PCI declines. T1_1 marks the transition from decline to growth, and T1_2 marks the reversal.	R^2=0.167, P < 0.05
		T2=0.51	At BBR=0.51, the growth rate of PCI peaks, indicating the strongest positive effect.	
BWR	PCI	T1_1=0.277, T1_2=0.516	Within BWR [0.277, 0.516], PCI increases; outside this range, PCI declines. T1_1 marks the transition from decline to growth, and T1_2 marks the reversal (or significant trend change).	R^2=0.167, P < 0.05
		T2=0.405	At BWR=0.405, PCI increases at the fastest rate.	

3.4 Cluster Analysis of Four Cooling Patterns

In this study, 120 park samples were classified into 4 cooling performance clusters by K-mean clustering algorithm (Table 7, Fig. 10), revealing the differences in cooling mechanisms among different park clusters.The High-Efficiency cluster (28 samples) with PCI=0.430, PCA=1.299, PCE=0.094 and PCD=1.288, presented a high-intensity, large-area, far-radial pattern. The dominant factors of this cluster are the increasing marginal utility interval of park area (PA) over 2.31 kΔand NDVI over 0.766. Among them, Qiandeng Lake Park and Wanglugang Forest Park achieve efficient cooling through the layout of large water bodies and high vegetation cover, respectively.

The Low-Efficiency cluster (48 samples) has negative cooling indicators (PCI=-0.733, PCA=-0.432, PCE=-0.184), and is characterised by short cooling distances and gentle gradient attenuation, which is mainly due to the high BD (BD>0.523) or insufficient FAR (FAR<7.986), and insufficient NDVI (NDVI<0.277). In particular, the Half Moon Island Wetland Park had a limited cooling effect due to a high ratio of impervious surfaces in the buffer zone.

The Moderate Efficiency cluster (39 samples) had a moderate PCI=0.594 but a significantly positive PCG=1.026, with negative PCA and PCI, reflecting outstanding spatial heterogeneity. The dominant factors were DEM (DEM<35.97 m) and microtopographic differences under artificial intervention. Among them, Zhongshan Park in Chancheng formed a strong cooling gradient due to its close proximity to the built-up area but failed to reach an efficient level due to its size. Comprehensive clusters (5 samples) with PCE=4.199 were extremely high, such as the high evapotranspiration agricultural wetland model in Shuiteng Park.

Table 7 Cooling Characteristics of Four Park Clusters

Cluster Name	Samples	PCI	PCA	PCE	PCD	PCG	Typical Cases
High-Efficiency	28	0.430	1.299	0.094	1.288	-0.695	Qiandeng Lake Park, Yingyue Lake Park, Wangjiegang Forest Park
Low-Efficiency	48	-0.733	-0.432	-0.184	-0.352	-0.341	Banyuedao Wetland Park, Nanhai National Fitness Sports Park
Moderate Efficiency	39	0.594	-0.487	-0.380	-0.706	1.026	Chancheng Zhongshan Park, Shiwan Park, Leigang Park
Comprehensive	5	0.000	0.673	4.199	1.671	-0.830	Yucun Cultural Park, Huahai Liuchao, Shuiteng Park

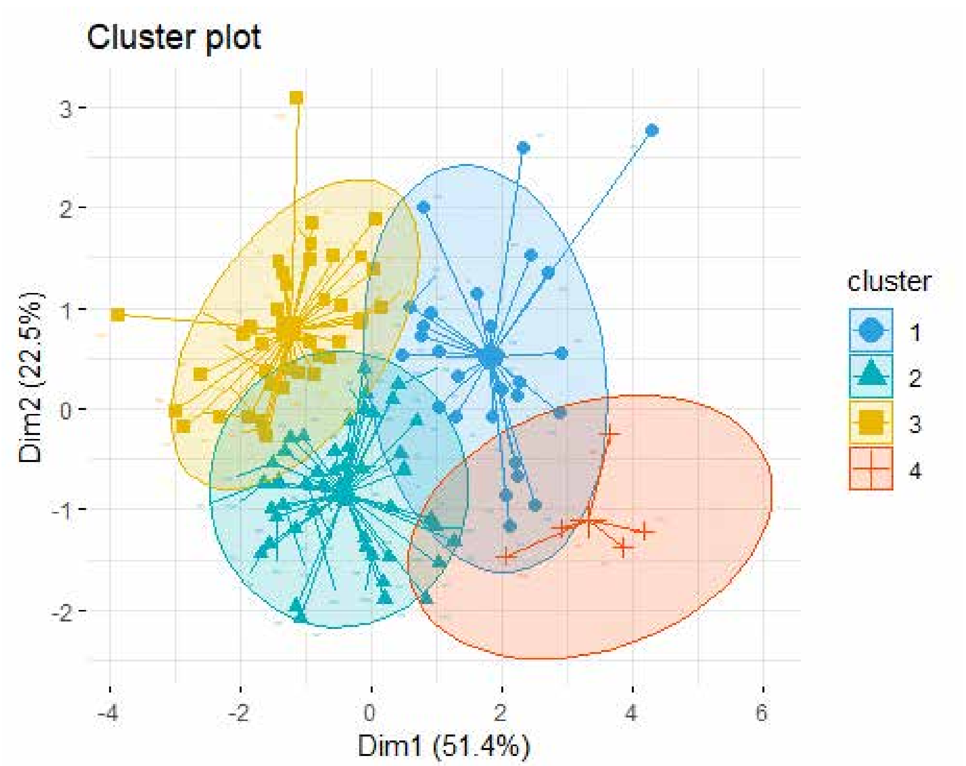

Figure 10 Cluster Diagram of Park Cooling Patterns Based on K-mean

4. Discussions

4.1Threshold Mechanisms for Heat Mitigation of Urban Parks in Water-Network Cities

The study reveals the nonlinear threshold relationship between the cooling performance of parks and key factors such as PA, NDVI, BD and BWR in water network cities, and constructs a methodological framework for the analysis of cooling performance indices and thresholds. The marginal utility of PA increases in the interval of [2.31, 4.03] km², which is a breakthrough from the traditional perception that the larger the size of the park, the better the cooling effect. It is proved that a moderate-sized park can achieve more efficient thermal mitigation by optimising the spatial layout. In addition, the decreasing and then increasing effect of NDVI with 0.277 as the turning point reveals the critical relationship between vegetation cover and cooling intensity. For the blue-green spatial indicators (BBR, BWR) of the buffer zone in the water network city, it was found that there was a threshold interval for the cooling effect. the PCI of BWR rose at [0.277, 0.516]. It provides a quantitative basis for the synergistic cooling of blue-green and enriches the thermal mitigation research on the coupling of urban ecohydrological elements.

4.2 Threshold-Based Planning Strategies

4.2.1 Hierarchical Control: Threshold Adaptation for Medium and High Efficiency Cooled Parks

For High-Efficiency Cooling Performance Parks (Cluster I), large parks with a PA greater than 2.31 km² and an NDVI greater than 0.766 should be strictly protected from fragmented development. For example, the Qiandeng Lake Park should maintain a balance between the thresholds of water body area and vegetation cover, and avoid the impervious surface ratio (BBR) of the buffer zone exceeding 0.188. For high-density built-up area parks (e.g., Wenhua Park) with BD greater than 0.523 or FAR less than 7.986 in Low-Efficiency Parks (Cluster II), the NDVI should be increased to 0.277 or above by removing walls to allow greening, vertical greening and other measures, while controlling the density of the new buildings to be ≤0.251 (Gill et al., 2007; Keeler et al., 2019)and changes to hydrology such as increased surface runoff of rainwater. Such changes are, in part, a result of the altered surface cover of the urban area. For example less vegetated surfaces lead to a decrease in evaporative cooling, whilst an increase in surface sealing results in increased surface runoff. Climate change will amplify these distinctive features. This paper explores the important role that the green infrastructure, i.e. the greenspace network, of a city can play in adapting for climate change. It uses the conurbation of Greater Manchester as a case study site. The paper presents output from energy exchange and hydrological models showing surface temperature and surface runoff in relation to the green infrastructure under current and future climate scenarios. The implications for an adaptation strategy to climate change in the urban environment are discussed.","container-title":"Built Environment (1978-. Moderate Efficiency parks (Cluster III) can use microtopography and artificial water bodies to optimise the cooling gradient, based on the PCG rise when the DEM is less than the 35.97 m threshold. For example, Zhongshan Park in Chancheng can make up for the lack of area by enhancing the temperature difference with the surrounding heat islands through the extension of the water system.

4.2.2 Spatial Optimization: Synergy between Blue and Green Networks

The blue-green network construction strategy based on horizontal and vertical threshold synergy provides a multi-dimensional spatial optimisation path for thermal environment management in water network cities. In terms of horizontal synergy, waterfront buffer zones with BWR ≥ 0.277 are combined with vegetation corridors with NDVI ≥ 0.277 in urban planning. A composite cooling chain is formed through the coupling of water evaporation and vegetation transpiration. Foshan Riverside Wetland Park enhances the PCI by 32% through the synergistic configuration of BWR=0.405 and NDVI=0.65. Secondly, vertical synergy, in the area of undulating terrain, the vegetation communities with staggered heights can be laid out. When the DEM was in the interval of 49.55-72.27 m, the effect of elevation on PCE showed a tendency of decreasing and then increasing. The cooling gradient is enhanced through the difference of transpiration in three-dimensional space. For example, the cooling efficacy of different elevation intervals was effectively enhanced by the vertical layering configuration of mountain vegetation in Wang Luegang Forest Park.

4.2.3 Optimization Strategies: Threshold Enhancement for Inefficient Parks

For the Low-Efficiency parks in cluster Δ the three-threshold priority transformation path requires systematic integration of ecological restoration and spatial planning strategies. Firstly, taking the green space threshold as the priority transformation guide, for the parks with NDVI<0.277, the vegetation cover is improved through high-density planting of native tree species, and the transformation target of NDVI≥0.4 is set. Native plants in Foshan City occupy an important position in urban greening, and the plan requires that no less than 70% of the plant species applied in urban greening are native species. For example, Ficus microcarpa, Ficus alpina, Camphor, Viburnum, Bombax, etc. are commonly used native species in Foshan.

At the same time, the buffer zone BBR control is limited to a threshold of 0.252, and measures such as softening of the hard interface are taken to weaken the heat-reflecting effect and enhance transpiration. Optimisation through density threshold. For the area around the park with a BD greater than 0.523, planning policy tools such as volume ratio transfer will guide the building setbacks to regulate the BD to a reasonable range of [0.251, 0.523], and release ventilation corridors to promote air circulation. By implementing water body threshold supplementation, for small green spaces with PA less than 2.31 km², raising BWR to above 0.277 by introducing micro water features such as fountains and rain gardens (Keeler et al., 2019) can increase PCI by 15-20%. This progressive intervention pathway can form a chain of inefficient park renovation techniques from ecological substrate restoration to spatial structure optimisation.

4.3 Validation and Comparative Analysis of Thresholds for Park Cooling Performance
This study validates research related to thermal mitigation in parks. It has been suggested that NDVI needs to exceed 30% for significant cooling (Gill et al., 2007). This study validates this conclusion through a threshold of 0.277 NDVI and refines the mechanism of the negative effect in the low-coverage zone. In contrast to the subtropical water network city study, this study quantified the inverted U-shaped relationship between BWR and PCI (T1_1=0.277, T1_2=0.516), which complements the explanation that excessive concentration of water bodies inversely leads to a decrease in cooling efficiency. In addition, the PA marginal utility intervals found in the study were highly consistent with the optimal scale of 2-5 km² for thermal mitigation in urban parks proposed by the U.S. Environmental Protection Agency (EPA) (Wong et al., 2021), further validating the universality of the thresholds.

4.4 Research Limitations and Future Directions
The limitations of the study are that the thresholds are based on remote sensing data from a single city in a single season, and their applicability in cities with significant differences in climate zones has to be verified. Second, socio-economic variables such as population density and energy consumption were not included, making it difficult to analyse the impact of human-environment interaction on cooling performance. In the future, we can expand the sample to more cities in the Yangtze River Delta and Pearl River Delta, and construct a cross-regional threshold model. The combination of UAV thermal imaging and ground-based measurements can improve the data accuracy, and the introduction of SD models to simulate the evolution of the thermal environment under the threshold regulation can provide a tool to support dynamic planning.

5. Conclusion
In the context of the global urban heat island effect dilemma, this study reveals the mechanism of urban heat mitigation by urban parks through multi-indicator assessment and machine learning modelling. This study found that high-intensity urban heat island environments attenuate the spatial decay rate of park cooling effects. The BRT model and RCS curves revealed that there are key thresholds for the core drivers: the optimal scale of heat mitigation in urban parks is 2.3-4 km²; the NDVI of parks needs to be over 27.7% to achieve significant cooling effect; the BWR has an inverted U-shape relationship with PCI, and the optimal blue spatial threshold is 40%. Finally, 120 parks were classified into four categories, High-Efficiency, Low-Efficiency, Moderate Efficiency and Comprehensive by K-means clustering algorithm. The study proposes targeted planning strategies for the four categories of parks, among which the low-efficiency parks can improve the cooling performance by increasing the vegetation cover and controlling the building density, and optimising the blue-green space layout. This study can provide useful guidance for the development of blue-green landscape spaces in water network cities to address global climate change.

Reference:

Books:
Elith, J., Leathwick, J., & Hastie, T. (2008). A working guide to boosted regression trees. *The Journal of Animal Ecology*, 77, 802–813.

V., Franch, B., Romaguera, M., Oltra-Carrió, R., Julien, Y., & Mattar, C. (2010). Obtención de la temperatura de la superficie terrestre a partir de la serie histórica LANDSAT. *Revista de Teledetección*, *33*, 53–63.

Journal article

Aram, F., Higueras García, E., Solgi, E., & Mansournia, S. (2019). Urban green space cooling effect in cities. *Heliyon*, *5*(4), e01339.

Bowler, D. E., Buyung-Ali, L., Knight, T. M., & Pullin, A. S. (2010). Urban greening to cool towns and cities: A systematic review of the empirical evidence. *Landscape and Urban Planning*, *97*(3), 147–155.

Chang, C.-R., & Li, M.-H. (2014). Effects of urban parks on the local urban thermal environment. *Urban Forestry & Urban Greening*, *13*(4), 672–681. https://doi.org/10.1016/j.ufug.2014.08.001

Feyisa, G. L., Dons, K., & Meilby, H. (2014). Efficiency of parks in mitigating urban heat island effect: An example from addis ababa. *Landscape and Urban Planning*, *123*, 87–95.

Friedman, J. H. (2001). Greedy function approximation: A gradient boosting machine. *The Annals of Statistics*, *29*(5), 1189–1232.

Gago, E. J., Roldan, J., Pacheco-Torres, R., & Ordóñez, J. (2013). The city and urban heat islands: A review of strategies to mitigate adverse effects. *Renewable and Sustainable Energy Reviews*, *25*, 749–758.

GALLO, K. P., McNAB ,A. L., KARL ,T. R., BROWN ,J. F., HOOD ,J. J., & and TARPLEY, J. D. (1993). The use of a vegetation index for assessment of the urban heat island effect. *International Journal of Remote Sensing*, *14*(11), 2223–2230.

Gill, S. E., Handley, J. F., Ennos, A. R., & Pauleit, S. (2007). Adapting cities for climate change: The role of the green infrastructure. *Built Environment (1978-)*, *33*(1), 115–133.

Gong, C., Yang, R., & Li, S. (2024). The role of urban green space in promoting health and well-being is related to nature connectedness and biodiversity: Evidence from a two-factor mixed-design experiment. *Landscape and Urban Planning*, *245*, 105020.

Govindarajulu, U. S., Malloy, E. J., Ganguli, B., Spiegelman, D., & Eisen, E. A. (2009). The comparison of alternative smoothing methods for fitting non-linear exposure-response relationships with cox models in a simulation study. *The International Journal of Biostatistics*, *5*(1).

Jimenez, J.-C., Sobrino, J., Cristóbal Rosselló, J., Sòria Barres, G., Ninyerola, M., Pons, X., Hidalgo,

Kanungo, T., Mount, D. M., Netanyahu, N. S., Piatko, C. D., Silverman, R., & Wu, A. Y. (2002). An efficient k-means clustering algorithm: Analysis and implementation. *IEEE Transactions on Pattern Analysis and Machine Intelligence*, *24*(7), 881–892.

Kayet, N., Pathak, K., Chakrabarty, A., & Sahoo, S. (2016). Urban heat island explored by co-relationship between land surface temperature vs multiple vegetation indices. *Spatial Information Research*, *24*(5), 515–529.

Keeler, B. L., Hamel, P., McPhearson, T., Hamann, M. H., Donahue, M. L., Meza Prado, K. A., Arkema, K. K., Bratman, G. N., Brauman, K. A., Finlay, J. C., Guerry, A. D., Hobbie, S. E., Johnson, J. A., MacDonald, G. K., McDonald, R. I., Neverisky, N., & Wood, S. A. (2019). Social-ecological and technological factors moderate the value of urban nature. *Nature Sustainability*, *2*(1), 29–38.

Masson-Delmotte, V., Zhai, P., Pirani, A., Connors, S. L., Péan, C., Berger, S., Caud, N., Chen, Y., Goldfarb, L., Gomis, M. I., Huang, M., Leitzell, K., Lonnoy, E., Matthews, J. B. R., Maycock, T. K., Waterfield, T., Yelekçi, Ö., Yu, R., & Zhou, B. (Eds.). (2021). *Climate change 2021: The physical science basis. Contribution of working group I to the sixth assessment report of the intergovernmental panel on climate change*. Cambridge University Press.

Oke, T. R., & Maxwell, G. B. (1975). Urban heat island dynamics in montreal and vancouver. Atmospheric Environment (1967), 9(2), 191–200. https://doi.org/10.1016/0004-6981(75)90067-0

Oliveira, S., Andrade, H., & Vaz, T. (2011). The cooling effect of green spaces as a contribution to the mitigation of urban heat: A case study in lisbon. Building and Environment, 46(11), 2186–2194. https://doi.org/10.1016/j.buildenv.2011.04.034

Rizwan, A. M., Dennis, L. Y. C., & Liu, C. (2008). A review on the generation, determination and mitigation of urban heat island. Journal of Environmental Sciences, 20(1), 120–128. https://doi.org/10.1016/S1001-0742(08)60019-4

Sobrino, J. A., Jiménez-Muñoz, J. C., & Paolini, L. (2004). Land surface temperature retrieval from LANDSAT TM 5. Remote Sensing of Environment, 90(4), 434–440.

Stewart, I. D. (2011). A systematic review and scientific critique of methodology in modern urban heat island literature. International Journal of Climatology, 31(2), 200–217.

Wong, N. H., Tan, C. L., Kolokotsa, D. D., & Takebayashi, H. (2021). Greenery as a mitigation and adaptation strategy to urban heat. Nature Reviews Earth & Environment, 2(3), 166–181.

Yang, G., Yu, Z., Jørgensen, G., & Vejre, H. (2020). How can urban blue-green space be planned for climate adaption in high-latitude cities? A seasonal perspective. Sustainable Cities and Society, 53, 101932.

Yu, X., Guo, X., & Wu, Z. (2014). Land surface temperature retrieval from landsat 8 TIRS—comparison between radiative transfer equation-based method, split window algorithm and single channel method. Remote Sensing, 6(10), Article 10.

Yu, Z., Guo, X., Jørgensen, G., & Vejre, H. (2017). How can urban green spaces be planned for climate adaptation in subtropical cities? Ecological Indicators, 82, 152–162.

Yu, Z., Yang, G., Zuo, S., Jørgensen, G., Koga, M., & Vejre, H. (2020). Critical review on the cooling effect of urban blue-green space: A threshold-size perspective. Urban Forestry & Urban Greening, 49, 126630.

Zhang, J., Zhang, H., & Qi, R. (2024). A study of size threshold for cooling effect in urban parks and their cooling accessibility and equity. Scientific Reports, 14(1), 16176.

Zhao, M., Zhou, Q., Luo, Y., Li, Y., Wang, Y., & Yuan, E. (2024). Threshold effects between ecosystem services and natural and social drivers in karst landscapes. Land, 13(5), Article 5.

Reports and other documents:

Foshan Municipal People's Government. (2025). The Overall Plan for the Territorial Space of Foshan City (2021—2035). https://www.foshan.gov.cn/zwgk/gggs/content/post_6275957.html

Ministry of Housing and Urban-Rural Development. (2020). Standard for Urban Green Space Planning. https://ndls.org.cn/standard/detail/7033784c989d39e93c3d469401e2a910

Acknowledgement

The study is supported by National Key R&D Program of China (2024YFF1307000); and Shanghai Municipal Science and Technology Innovation Action Plan (22dz1202604).